

## MIT Open Access Articles

*An acoustic remote sensing method for high-precision propeller rotation and speed estimation of unmanned underwater vehicles*

The MIT Faculty has made this article openly available. **Please share** how this access benefits you. Your story matters.

**Citation:** Kristen Railey, Dino DiBiaso, Henrik Schmidt; An acoustic remote sensing method for high-precision propeller rotation and speed estimation of unmanned underwater vehicles. J. Acoust. Soc. Am. 1 December 2020; 148 (6): 3942–3950.

**As Published:** 10.1121/10.0002954

**Publisher:** Acoustical Society of America

**Persistent URL:** <https://hdl.handle.net/1721.1/154271>

**Version:** Final published version: final published article, as it appeared in a journal, conference proceedings, or other formally published context

**Terms of Use:** Article is made available in accordance with the publisher's policy and may be subject to US copyright law. Please refer to the publisher's site for terms of use.



DECEMBER 23 2020

## An acoustic remote sensing method for high-precision propeller rotation and speed estimation of unmanned underwater vehicles

Kristen Railey; Dino DiBiaso; Henrik Schmidt



*J. Acoust. Soc. Am.* 148, 3942–3950 (2020)

<https://doi.org/10.1121/10.0002954>



LEARN MORE

Advance your science and career as a member of the  
**Acoustical Society of America**

# An acoustic remote sensing method for high-precision propeller rotation and speed estimation of unmanned underwater vehicles

Kristen Railey,<sup>1,a)</sup> Dino DiBiaso,<sup>2</sup> and Henrik Schmidt<sup>1</sup>

<sup>1</sup>*Department of Mechanical Engineering, Massachusetts Institute of Technology, 77 Massachusetts Avenue 5-204, Cambridge, Massachusetts 02139, USA*

<sup>2</sup>*Systems Engineering, Draper, 555 Technology Square, Cambridge, Massachusetts 02139, USA*

## ABSTRACT:

Understanding the dominant sources of acoustic noise in unmanned underwater vehicles (UUVs) is important for passively tracking these platforms and for designing quieter propulsion systems. This work describes how the vehicle's propeller rotation can be passively measured by the unique high frequency acoustic signature of a brushless DC motor propulsion system and compares this method to Detection of Envelope Modulation on Noise (DEMON) measurements. First, causes of high frequency tones were determined through direct measurements of two micro-UUVs and an isolated thruster at a range of speeds. From this analysis, common and dominant features of noise were established: strong tones at the motor's pulse-width modulated frequency and its second harmonic, with sideband spacings at the propeller rotation frequency multiplied by the poles of the motor. In shallow water field experiments, measuring motor noise was a superior method to the DEMON algorithm for estimating UUV speed. In negligible currents, and when the UUV turn-per-knot ratio was known, measuring motor noise produced speed predictions within the error range of the vehicle's inertial navigation system's reported speed. These findings are applicable to other vehicles that rely on brushless DC motors and can be easily integrated into passive acoustic systems for target motion analysis. © 2020 Acoustical Society of America. <https://doi.org/10.1121/10.0002954>

(Received 9 July 2020; revised 17 November 2020; accepted 2 December 2020; published online 23 December 2020)

[Editor: Aaron M. Thode]

Pages: 3942–3950

## I. INTRODUCTION

In the past decade, unmanned underwater vehicle (UUV) technology has significantly improved in the areas of navigation, sensing, and autonomy. With new developments in navigation, UUVs have become capable of traveling under moving ice, which was previously considered an impossible task, giving scientists critical data to understand climate change in ice-covered seas.<sup>1</sup> During Deepwater Horizon, vehicles equipped with multi-sensor packages, including a mass spectrometer, were used to assess the impact of oil spills.<sup>2</sup> Research in optimal path planning and swarm cooperation has enabled vehicles to efficiently collect environmental data on large spatial and temporal scales in the ocean, which has been critical for weather modeling.<sup>3</sup> In defense applications, UUVs have historically played a role in mine countermeasures. With advancing technology, UUVs are tracking submarines with active sonar,<sup>4</sup> surveilling the ocean for intelligence missions with optimal path planning for energy consumption and avoidance of fishing nets,<sup>5</sup> and strategically delivering mines, which requires precise navigation.<sup>6</sup> The vehicles are performing more offensive missions, and so countering UUVs from acting on their malicious intent has become a new national security

priority.<sup>7–9</sup> Existing passive acoustic defense systems are challenged by detecting and tracking these vehicles.

In general, passive acoustic monitoring (PAM) is important for a range of applications, from surveilling marine protected areas to harbor security. PAM applied to the radiated noise of vessels—ships,<sup>10–12</sup> submarines,<sup>13</sup> and torpedoes<sup>14</sup>—and even divers<sup>15–17</sup> has been thoroughly investigated. As discussed in Urlick,<sup>14</sup> the prominent sources of radiated noise in vessels are machinery and propeller noise, which can be analyzed for classifying the target and estimating target speed. The continuous spectrum of propeller cavitation noise is amplitude modulated at the propeller shaft rotation speed or at the propeller blade rate frequency. A method to identify these fundamental frequencies and their harmonics is the DEMON (Detection of Envelope Modulation on Noise) algorithm.<sup>10,11,18,19</sup> In the low frequency domain, propeller noise also consists of discrete spectral components at the blade rate frequency and its harmonics.<sup>14</sup> Identifying small boat signatures in noisy environments by applying DEMON analysis and measuring low frequency blade lines has been demonstrated.<sup>10–12</sup> For submarines, Dixon *et al.* discusses the directivity pattern of the blade rate sound and how the unique turn-per-knot ratio (mapping of the rotational speed of the propeller to the underway speed) of a vessel can be used for estimating speed.<sup>13</sup>

<sup>a)</sup>Also at: Woods Hole Oceanographic Institution, Woods Hole, MA 02543, USA. Electronic mail: [krailey@mit.edu](mailto:krailey@mit.edu)

When using this method in practice for classifying and tracking UUVs, one must consider some important aspects of propeller noise that affect the DEMON algorithm performance and differ from machinery noise: the characteristic radiation pattern is weaker in the fore-and-aft directions, and the SNR strongly depends on speed and depth.<sup>14</sup> Another challenge for DEMON analysis is the selection of the propeller noise passband filter, which can significantly affect the algorithm's performance. The ideal passband filter varies widely between vessels and is chosen generally based on trial and error.<sup>11</sup> Passively tracking vessels by low frequency blade lines and propeller noise is challenging in a noisy and dynamic environment such as the shallow waters of harbors. Harbors are rich with noise sources: pile driving, ship traffic, motor vehicle traffic on nearby bridges, and construction. The cutoff frequency for a shallow water duct should also be taken into consideration.

Passively detecting and tracking UUVs from DEMON spectra, and more generally, radiated noise, is a relatively unexplored research area in comparison to other marine vessels. There has been an initiative (summarized in Holmes *et al.*) to understand and mitigate unwanted noise in mid- to low-frequencies (below 10 kHz) that interferes with onboard acoustic sensors.<sup>20</sup> The authors discuss how the field fluctuations in the magnetic pole gap between the stator and rotor inside a motor lead to significant monopole vibration of the motor housing.<sup>20</sup> In the field, Gebbie *et al.* analyzed the angular dependence of radiated noise from an underway REMUS-100 UUV via a bottom-mounted horizontal line array in a quiet ocean environment.<sup>21</sup> The authors were able to track the UUV by a single tone of 1065 Hz, which they attributed to originate from the propulsion system. Zhang *et al.* discussed how the Doppler effect on symmetric spectral lines around the switching frequency of an inverter-fed motor can be measured to estimate radial velocity.<sup>22</sup> However, previous work in radiated noise of UUVs does not pinpoint the causes of spectral noise to the vehicle's motor design parameters or estimate the speed of the vehicle.

In order to isolate and characterize motor noise, we focus on brushless DC (BLDC) motors because they are prevalent in UUV propulsion systems—including the REMUS-100/600/6000, Sentry, Iver2, Dorado-class,<sup>23</sup> and Autosub<sup>24</sup>—for their reliability, efficiency, and low-noise.<sup>25</sup> Various design aspects of these motors—the pole number, motor operating frequency, the pulse-width modulated (PWM) switching frequency ( $f_{\text{PWM}}$ ), and the natural mechanical vibration modes of the whole system—contribute to strong tonal acoustic features.<sup>26</sup> Several groups have confirmed through experimentation and modeling that  $f_{\text{PWM}}$  and its harmonics, especially  $2f_{\text{PWM}}$ , are dominant sources of noise.<sup>26–32</sup> In general, to address noise mitigation in motors, several techniques include reducing cogging torque ripple through magnetic pole design,<sup>33</sup> randomized PWM,<sup>34</sup> and modifying the commutation sequence.<sup>35</sup> However, these design changes are not without tradeoffs. Islam *et al.* points out that for the mass-manufactured BLDC motor, minimizing cogging torque ripple increases overall cost, complexity

of the stator and rotor magnet construction, as well as the potential loss of output torque. Lo *et al.* summarizes limitations of altering  $f_{\text{PWM}}$  to reduce noise. A randomized PWM signal, which results in flat, broadband noise, may eliminate a strong tone but then increase the probability of aligning with other mechanical resonances. For some applications, it is sufficient to move  $f_{\text{PWM}}$  outside of the audible range. However, increasing  $f_{\text{PWM}}$  leads to higher switching loss in the metal–oxide–semiconductor field-effect transistors (MOSFETs).<sup>26</sup>

Building off of previous work in both UUV and BLDC motor noise, we describe a passive acoustic, high precision method for estimating the micro-UUV's propeller rotation frequency, which outperformed the DEMON algorithm in field experiments with highly variable noise and shallow water. Although the analysis of this work is focused on micro-UUVs, this method applies to other robotic platforms that are powered by mass-manufactured BLDC motors. First, the acoustic signatures of the two micro-UUVs (Sec. III A) and an isolated thruster (Sec. III B) were measured, and DEMON analysis performed. From this analysis, the sources of noise from the BLDC motor inside the propulsion systems are identified. Measuring the motor noise as a method for estimating UUV propeller speed was evaluated in field experiments with the two micro-UUVs (Sec. III D).

## II. METHODOLOGY

### A. Overview of the Sandshark and Riptide micro-UUVs

The BAE Systems Riptide (Mk1 version) and the General Dynamics Mission Systems Bluefin Sandshark micro-UUVs, pictured in Fig. 1, were selected for study. The tail-cone section of the Sandshark consists of a thruster, fin actuators, battery, altimeter, and inertial navigation system (INS). For propulsion, the thruster includes a motor controller and BLDC motor (Anaheim Automation BLWR173S-24V-2000) that operates with a PWM frequency between 15 and 20 kHz and 8 poles, producing a top speed of 2.5 m/s. The vehicle dynamics for pitch, roll, and heading are controlled by three fins actuated by a BLDC servomotor (Maxon EC-max 16), which is commanded by a PWM signal. The Riptide vehicle has a similar configuration as the Sandshark, but a notable difference is its reported top speed of 10 kts or 5.14 m/s. The thruster consists of a BlueRobotics M200 motor, which is a BLDC 3-phase motor. The BlueRobotics Basic 30 A ESC controller (r1) creates a 3-phase, PWM signal to power the motor at the desired rotations per minute. This PWM frequency is at 17 857 Hz. To isolate acoustic noise related to the motor, the BlueRobotics T200 thruster (electronic speed controller, BLDC motor, and propeller) was measured separately from the entire UUV system. This thruster was selected because the Riptide propulsion system is powered by an earlier version of this motor. In this updated version, the T200 motor is a brushless outrunner BLDC motor with 14 permanent magnetic poles on the rotor and 12 stator coils. This



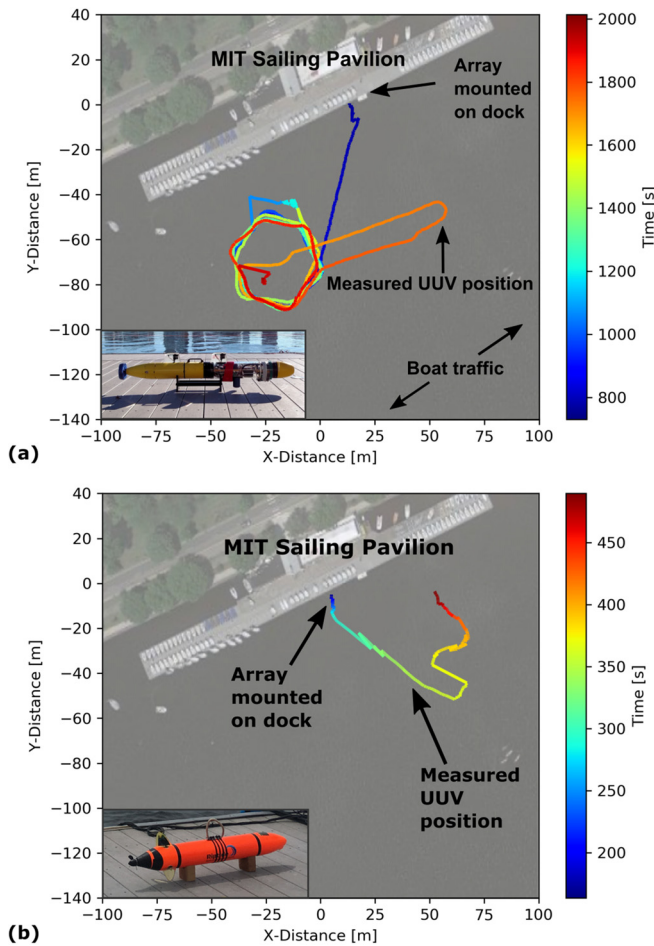


FIG. 1. (Color online) During field experiments with the (a) Sandshark and (b) Riptide UUVs, acoustic data was collected from the MIT Sailing Pavilion in the Charles River. The vehicle position over time, plotted here, was logged by the INS.

motor is controlled with the BlueRobotics Basic ESC (r3), which operates with a PWM frequency of 24 kHz.

### B. Identifying UUV acoustic features

The acoustic signatures of the two micro-UUVs were separately measured on an off-board hydrophone array (HTI-96-MIN,  $-165$  dB re.  $1$  V/  $\mu$ Pa hydrophones, which were also used in the subsequent experiments) in a quiet, controlled environment at a MIT campus swimming pool. In order to derive the acoustic signature of the UUV, the power spectral density (PSD) was estimated from time series acoustic data collected on a single hydrophone element in the line array using Welch's method<sup>36</sup> with a Hann window, segments of  $1$  s (and  $0.5$  s for the field tests), and  $50\%$  overlap. During the experiment, the vehicle was secured in place and the propeller rotated at different speeds for  $30$  s. Following the speed data collection, the thruster was off, and the fins moved a prescribed five degrees each five seconds. The sampling rate of the array was  $60\,060$  Hz. The measured motor tones that are above the Nyquist frequency have the subscript, "aliased." For example, the true  $2f_{\text{PWM}}$  is measured as  $2f_{\text{PWM,aliased}}$ . This process was repeated for both

the Sandshark and Riptide UUVs. At the MIT Towing Tank facility, the UUV thruster isolation experiment was performed in a tank, where the system was bottom-mounted, and acoustic measurements were taken off-board.

For each of these experiments, DEMON measurements were calculated using a  $10$ – $25$  kHz fifth-order Butterworth bandpass filter to capture the propeller noise. The amplitude envelope was determined by the magnitude of the Hilbert transform applied to the bandpass filtered signal. The amplitude envelope was downsampled to  $1000$  Hz, using the root mean square (RMS) method described in Chung *et al.*<sup>10</sup> Finally, the DEMON spectrum was calculated from the FFT of the amplitude envelope.

### C. Speed and propeller rotation measurement method

The relationship between strong acoustic tones emitted by the propulsion system and the rotations per minute of the thruster was determined experimentally. When the turn-per-knot ratio was known, as in the case of the Sandshark, vehicle speed was determined from the acoustic measurements. We verified that there is a strong tone at the  $f_{\text{PWM}}$  of the motor, which acts as a carrier to sidebands of spacing  $f_m$ , equal to the rotation frequency of the motor,  $f_s$ , multiplied by the number of permanent magnetic poles in the motor,  $p$ :

$$f_m = f_s p. \quad (1)$$

The resulting sidebands center around  $f_{\text{PWM}}$ :  $f_{\text{PWM}} \pm k f_m$  and  $f_{\text{PWM}} \pm n f_s$ , where  $k$  and  $n$  are the respective harmonic orders. The first order of  $k$  dominates,  $f_{\text{PWM}} \pm f_m$ . Therefore, the measured sidebands can be used to predict  $p$  for classification and  $f_s$  for speed estimation. With DEMON analysis, where  $f_m$  is the dominant tone and  $f_s$  is also present, these values can be verified. In practice, the sideband values were measured through peak-finding and symmetry, and validated by the DEMON measurement results.

### D. Demonstration of speed estimation in field experiments

With knowledge of the motor acoustic features identified in the pool and tank, field experiments were completed in the Charles River of Boston, MA (approximately  $6$  m deep), to evaluate motor noise as a remote speed estimation method. Two experiments were performed: the Sandshark UUV test on October 31, 2016, and the Riptide UUV test on August 29, 2019. In both experiments, the hydrophone array was mounted to the MIT Sailing Pavilion dock, and the vehicle performed an autonomous mission, programmed with MOOS-IvP autonomy software.<sup>37</sup> A birds-eye view of both experiments is in Fig. 1. For the Sandshark test, the river current was insignificant and therefore not accounted for in estimating vehicle speed. Taken from the vehicle's INS, the average vehicle depth and speed were, respectively,  $1.90 \pm 0.26$  m and  $1.354 \pm 0.098$  m/s. In comparison, for the Riptide test, the robot's average depth and speed were:  $-0.123 \pm 0.13$  m (at the surface) and  $0.835 \pm 0.452$  m/s.

The array sampling rates for the Sandshark and Riptide experiments were 37 500 and 60 060 Hz, respectively. The sideband spacing measurement error is reported as half of the peak width at half the height of the peak's prominence.

### III. RESULTS

#### A. Sandshark UUV acoustic signature

To identify acoustic features of the Sandshark UUV, vehicle noise data was collected at different speeds (400 rpm, 800 rpm, and 1000 rpm) for 30 s time intervals, followed by isolated fin movements. The spectrogram of the

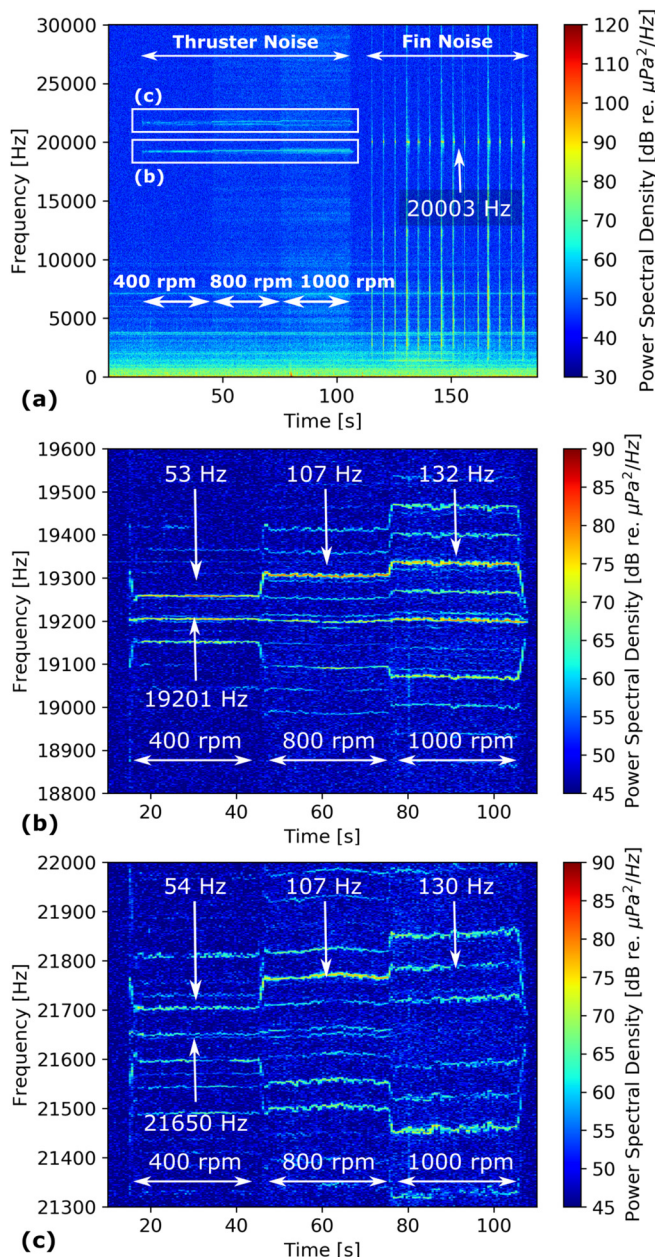


FIG. 2. (Color online) (a) The radiated noise from a Sandshark UUV was characterized at different speeds, followed by isolated fin movements. Three features are highlighted: (b) a constant tone at 19 201 Hz, which matches  $f_{\text{PWM}}$ , and lastly (b)-(c), sideband spacings that increase with speed (c) a tone at  $2f_{\text{PWM,aliased}}$ .

entire experiment in Fig. 2(a) highlights two distinct tones that are then magnified in Figs. 2(b) and 2(c). The tones, 19 201 and 21 650 Hz, are dominant and constant over all speeds. Based off of previous work in characterizing motor noise<sup>26–32</sup> and the motor specifications of the vehicle, we infer that these tones correspond to  $f_{\text{PWM}}$  and its multiple,  $2f_{\text{PWM,aliased}}$ . The observed tone is close to the manufacturer provided range for the  $f_{\text{PWM}}$  of this specific motor: 15–19 kHz. In addition, the measured signal, 21 650 Hz, is a 0.04% percent error of the expected value for  $2f_{\text{PWM,aliased}}$ . Sideband frequency intervals, which correspond to  $f_m$ , are centered around the carrier  $f_{\text{PWM}}$ , [Fig. 2(b)] and its second multiple,  $2f_{\text{PWM,aliased}}$  [Fig. 2(c)]. To illustrate these observed acoustic features at a single speed, the PSD for 400 rpm, is centered at 19 205 Hz in Fig. 3(a) and at 21 650 Hz in Fig. 3(b) (the respective center tones for this speed specifically). Grey lines are drawn at the expected sideband values of  $f_m$  or  $pf_s$ . Additional sidebands are observed at  $f_s$ , as labelled in Fig. 3(a). The DEMON spectrum for this speed in Fig. 3(c) agrees with the motor noise: there is a strong tone at  $f_m$  and its second multiple. Following the vehicle speed acoustic measurements, the sound of fin movement was characterized. There are two main fin noise tones that are observed at 20 003 Hz [labelled in Fig. 2(a)] and 20 053 Hz, which we attribute to  $f_{\text{PWM}}$  and  $2f_{\text{PWM,aliased}}$ .

#### B. Riptide UUV and T200 thruster acoustic signatures

For the Riptide UUV noise characterization experiment, the vehicle was programmed to increase its desired speed in 30 s time intervals from 1 m/s to 5 m/s. As shown in the spectrogram in Fig. 4(a) across all five speeds, a tone is observed at 17 898 Hz, which is within a 0.23% percent error of the manufacturer specified  $f_{\text{PWM}}$ . Sidebands on this center tone correspond to  $f_m$ , which is verified by performing DEMON analysis in Fig. 4(b). In addition, there is a strong and consistent tone at 24 270 Hz that we attribute to be  $2f_{\text{PWM,aliased}}$ . For the desired speed of 1 m/s, the PSD is centered at  $f_{\text{PWM}}$  in Fig. 3(d) and at  $2f_{\text{PWM,aliased}}$  in Fig. 3(e). Grey lines are drawn to demonstrate how the sidebands align with  $f_m$  or  $pf_s$ . The DEMON spectrum of this speed in Fig. 3(f) supports the observation that  $f_m$  is a dominant tone. The additional sideband intervals that are observed in Figs. 3(d)–3(f) correspond to the fundamental motor rotation frequency,  $f_s$ .

To support the conclusions on the sources of acoustic noise from the BLDC motor in the two micro-UUVs, a motor isolation experiment was performed. Figure 5 is a spectrogram of this experiment, where the propellor rotational speed increased in time intervals of 30 s. As predicted, the motor emits two tones at  $f_{\text{PWM}}$  and  $2f_{\text{PWM}}$ , as well as sideband spacings that align with  $f_m$ . For all speeds, a steady tone at 24 008 Hz is observed that corresponds to the manufacturer specified  $f_{\text{PWM}}$  of the motor with 0.033% percent error. In addition, the measured value of  $2f_{\text{PWM,aliased}}$  is 12 044 Hz, exactly matching the expected value.



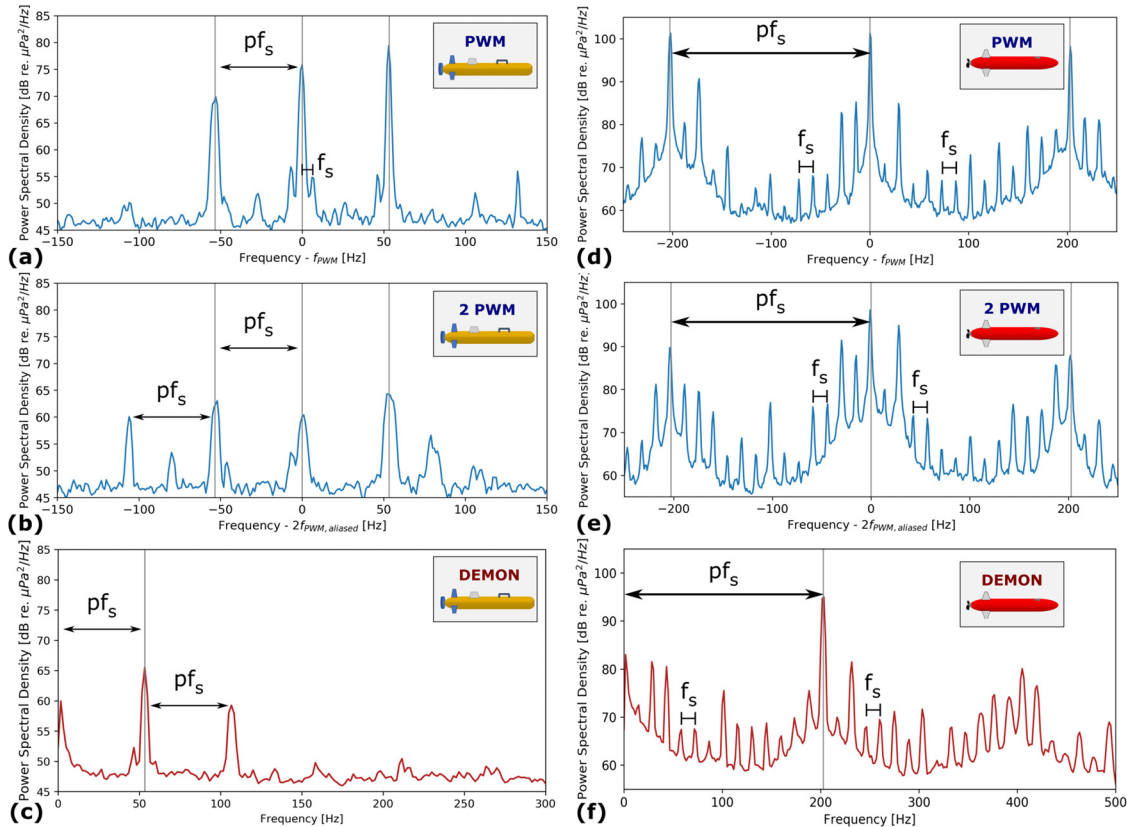


FIG. 3. (Color online) The radiated noise of the Sandshark at 400 rpm and the Riptide at approximately 870 rpm (1 m/s desired speed) are characterized in plots (a)–(c) and (d)–(f), respectively. The PSD plots are centered at  $f_{PWM}$  and  $2f_{PWM,aliased}$ , which are: (a) 19 205 Hz, (b) 21 650 Hz, (d) 17 884 Hz, and (e) 24 292 Hz. The DEMON spectrum is plotted in (c) and (f). Grey lines indicate  $pf_s$  and the spacing of  $f_s$  is annotated.

### C. Field measurements of UUV acoustic features

With insight into the acoustic spectral features of micro-UUVs, this information is used to demonstrate that the speed of the Riptide and Sandshark vehicles can be passively identified in the field under realistic conditions. In the spectrogram of the Sandshark experiment in Fig. 6(a), there are two prominent features that we match to the pool measurements of the UUV after accounting for aliasing: a tone at 18 270 Hz corresponds to  $f_{PWM,aliased}$  of the thruster with sidebands spaced by 142 Hz ( $f_m$ ), and a tone at 17 504 Hz corresponds to the  $f_{PWM,aliased}$  of the fin servomotors. As illustrated in Fig. 6(b), the navigation data also supports this conclusion: when the vehicle is underway, the thruster is on and tonal features ( $f_{PWM,aliased}$  and  $f_m$ ) are present. The consistent SNR of the radiated UUV noise while the robot loitered in a circle (about 15 dB and 45 dB above the background noise for the thruster and fin noise, respectively) indicates that the motor noise may be omni-directional. Also, when a boat passes, such as the time after 1600 s, the fin motor noise is still observable (about 10 dB above the background noise).

Acoustic features observed in the Riptide field experiment also aligned with characteristics identified in the pool test: a strong tone at  $f_{PWM}$  and  $2f_{PWM}$ , and sidebands of spacing  $f_m$ . As noted in the spectrogram in Fig. 7(a), there is a consistent tone at 17 890 Hz when the vehicle is underway,

which matches the measured  $f_{PWM}$  from the pool (0.045% percent error). A second tone at 24 264 Hz aligns with the expected value of  $2f_{PWM,aliased}$ . Sideband spacings of 212 Hz, corresponding to  $f_m$  are centered on the carrier frequency when the desired speed is 1 m/s. The sideband spacing increases to 251 Hz when the vehicle changes its desired speed to 1.5 m/s. Figure 7(c) shows the desired and actual speed of the vehicle from the INS. Dashed black lines illustrate how the vehicle speed aligns with the radiated acoustic noise. The depth of the vehicle was not included in the navigation plot because the vehicle was on the surface for this exercise. To show how the high frequency motor noise compares to the propeller cavitation noise, the DEMON spectrum is plotted in Fig. 7(b). The annotated tones of 212 Hz, 424 Hz, and 251 Hz correspond to  $f_m$ , matching the sideband spacings in Fig. 7(a). These features are more challenging to observe in the DEMON spectrum (about 15 dB above the background noise) and at times, such as between 340 and 360 s, not observable. The change in SNR could be explained by the characteristic radiation pattern of the propeller noise. For example, the vehicle starts by traveling at a constant heading, away from the dock (see Fig. 1), and the tonal features in the DEMON spectrum fade away until the vehicle changes direction at around 360 s. The motor noise has minimal variation and appears to be omni-directional (at about 30 dB above the background noise). The motor

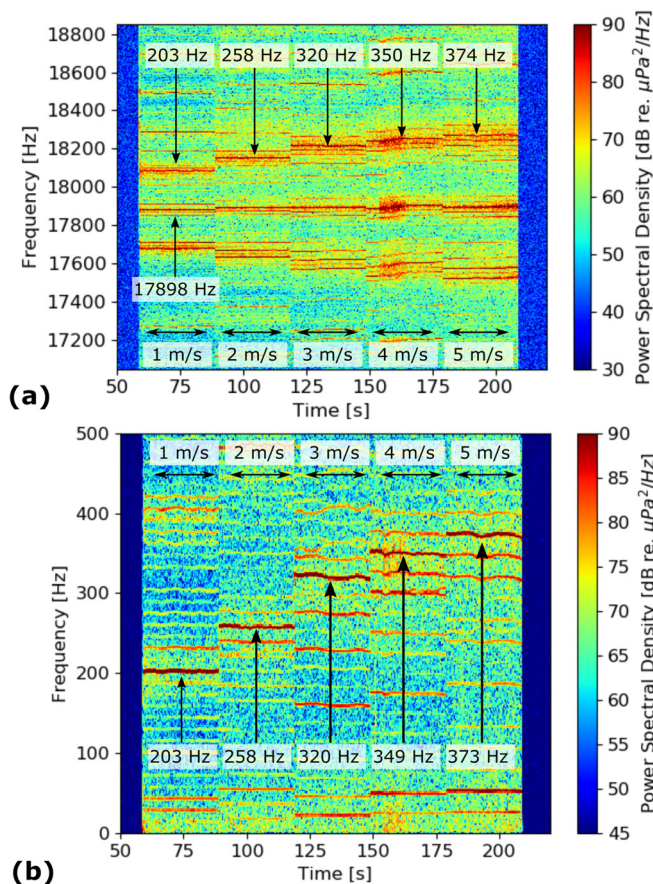


FIG. 4. (Color online) (a) A spectrogram of the Riptide UUV noise characterization test is centered at  $f_{PWM}$ . (b) The DEMON spectrum is plotted below. Sideband spacings in (a) correspond to the tones in (b).

noise is also observable when a boat passes, about 10 dB above the background noise, while the DEMON spectrum is dominated by the interfering boat's cavitation noise.

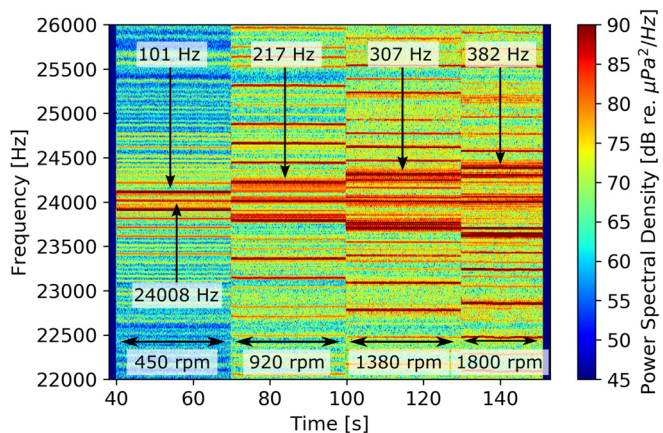


FIG. 5. (Color online) The spectrogram of the T200 motor isolation experiment is centered at 24 008 Hz ( $f_{PWM}$ ). As the speed increases, sidebands centered around the  $f_{PWM}$  carrier increase their interval spacing.

#### D. Derivation and field demonstration of speed and propeller rotation estimation method

To quantify the relationship between acoustic noise and vehicle speed, three different acoustic characterization experiments are compared—the Sandshark UUV, Riptide UUV, and T200 thruster—which involved BLDC motors of different specifications. The  $f_{PWM}$  and number of permanent magnetic poles,  $p$ , varies for the motor inside each of these systems. Therefore, as described in this section, we were able to verify the linear relationship of Eq. (1) between the rotational speed of the motor,  $f_s$ , and the sidebands with frequency intervals of  $f_m$ , centered on  $f_{PWM}$ . Also in this section, we show that the acoustic field measurements of an underway UUV can be used to extrapolate the vehicle speed by measuring the sidebands.

For the T200 thruster test, the measured sideband spacings,  $f_m$ , are plotted against the motor's corresponding

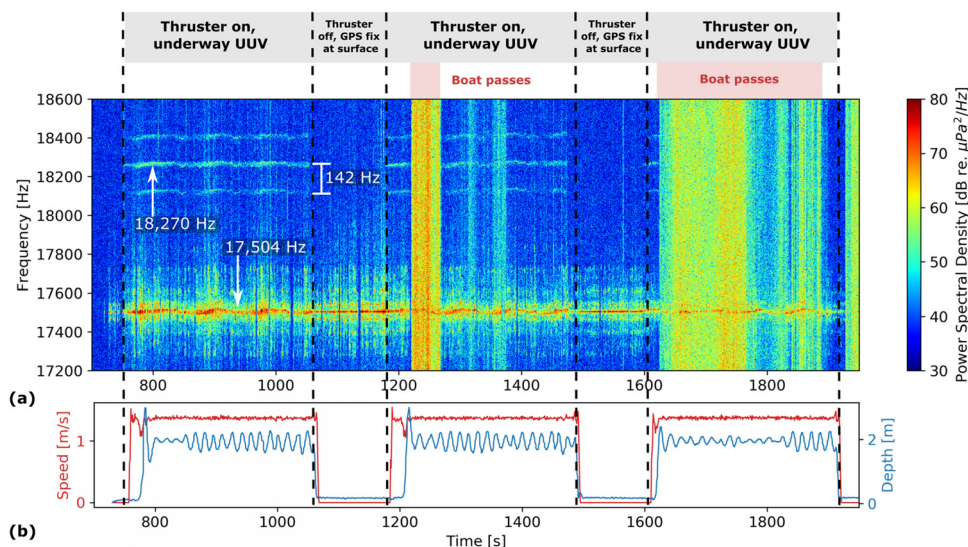


FIG. 6. (Color online) (a) The spectrogram of acoustic data from the Sandshark noise experiment in the Charles River is compared to (b) the vehicle navigation data. The tone at 18 270 Hz with sideband spacing at 142 Hz and the tone at 17 504 Hz correlate to the PWM switching frequencies of the thruster motor and fin servomotors. The former tone is present when the vehicle is underway.



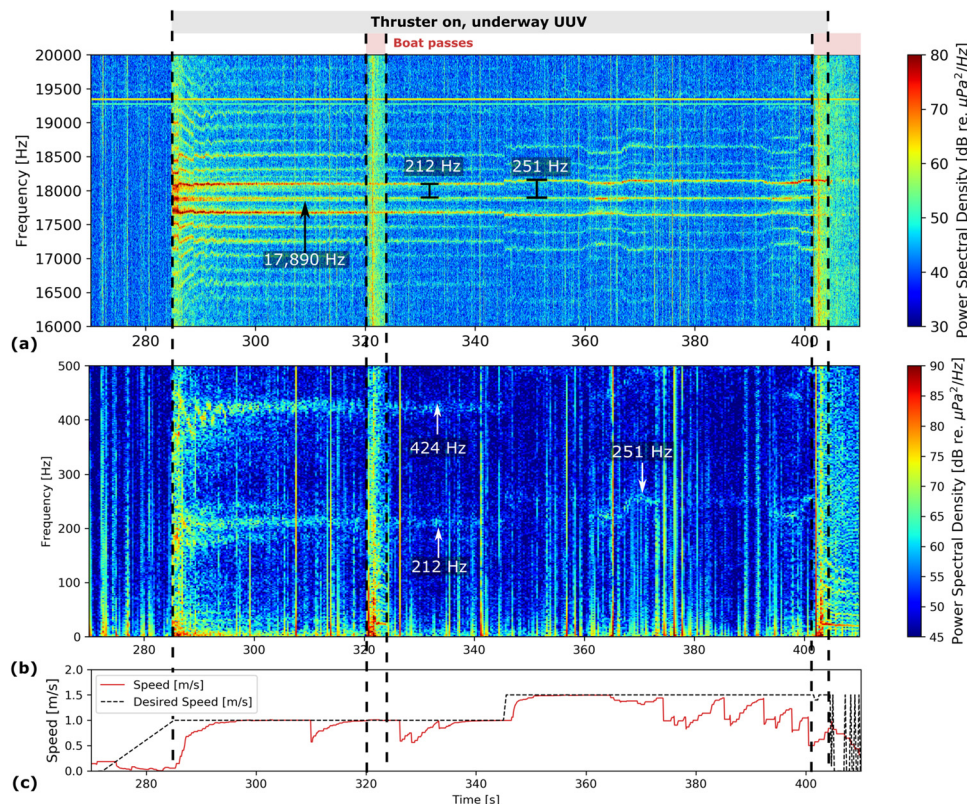


FIG. 7. (Color online) (a) The spectrogram of acoustic data from the Riptide noise experiment in the Charles River is compared to (b) the DEMON spectrum and (c) the vehicle navigation data from the INS of desired and actual speed. In (a), the constant tone at 17 890 Hz corresponds to  $f_{PWM}$  with sideband spacings of  $f_m$  at 212 Hz, which increase to 251 Hz with a desired speed change. The values of  $f_m$  are also present in (b).

speeds in Fig. 8(a). Applying a linear fit, the estimated pole number from the acoustic measurements was 13.1 (the true number of poles is 14). At the time of the Riptide UUV noise experiment, we did not have access to the true  $f_s$  mapping to the UUV desired speed that was used for programming the vehicle. Therefore, in Fig. 8(b), the measured sideband spacings from the pool experiment are plotted over the desired speed of the robot, and a second order fit is applied. The sideband spacing values of 212 and 251 Hz from the field are also plotted to show how well this relationship could predict the speed of the vehicle. The estimated speeds were 1.15 m/s and 1.69 m/s, which resulted in a percent error of 15.4% and 12.8%, respectively, compared to the true desired speed. The pool experiment results of the Sandshark UUV sideband spacing values,  $f_m$ , at three different speeds are plotted in Fig. 8(c). Given the number of poles in the Sandshark thruster motor (8 poles), the predicted values of  $f_m$  from Eq. (1) were plotted. The estimated pole number from the acoustic measurements is 7.96. To demonstrate that this relationship can predict the speed of an underway vehicle with a known turn-per-knot ratio in negligible currents, we consider the period of 770 s to 1035 s in the Sandshark field experiment. The vehicle speed for this time segment, reported by the INS of the robot was  $1.36 \pm 0.04$  m/s or  $1079 \pm 29$  rpm [drawn in Fig. 8(c)]. The measured sideband spacing for this segment was  $142 \pm 6$  Hz. From Eq. (1), with the known pole number of 8, the

expected value of the vehicle speed is  $1.34 \pm 0.08$  m/s or  $1065 \pm 32$  rpm, which is within the error range of the INS reported vehicle speed and yields a 1.3% error of the rpm measurement, using the INS value as truth. Therefore, with this insight into the relationship between  $f_m$  and  $f_s$ , we demonstrate that the speed of the Sandshark UUV can be estimated in the field by measuring the sidebands.

#### IV. CONCLUSION

In this work, a method for passively estimating the propeller rotation ( $f_s$ ) and speed of a UUV is derived and evaluated through experimentation, and compared to the DEMON algorithm. The acoustic signatures of two micro-UUVs, the Sandshark and Riptide, were measured at a range of speeds to pinpoint sources of spectral noise. To isolate noise emitting from the propulsion system, the T200 thruster was also characterized. From these experiments, we determined that the PWM switching frequency,  $f_{PWM}$ , and its multiple,  $2f_{PWM}$ , of the modulated voltage signal that drives the BLDC motor in these propulsion systems are dominant sources of acoustic noise. In addition, there are sidebands of spacing,  $f_m$  (the prominent sideband value) and  $f_s$ , that are centered around  $f_{PWM}$ . We validated, through experimentation, that the sideband spacing of  $f_m$  is equal to  $f_s$  multiplied by the number of permanent magnetic poles,  $p$ , in the motor [Eq. (1)]. When the sideband spacing of  $f_s$  is also present in the motor noise signature,  $p$  can be determined.

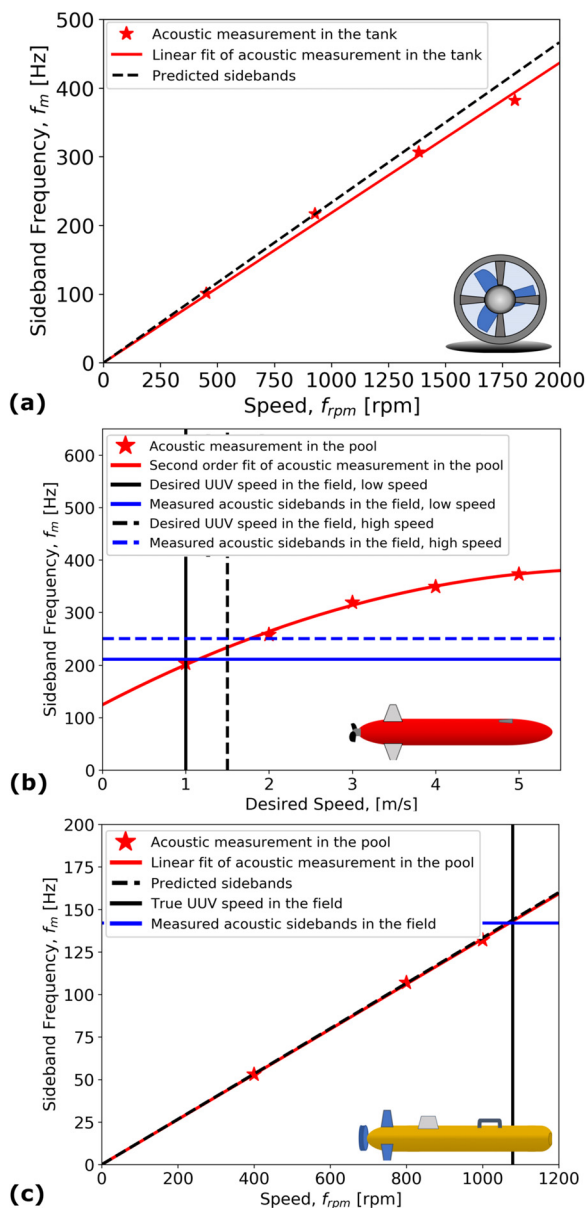


FIG. 8. (Color online) The acoustic measurements of the sideband frequency intervals,  $f_m$ , are compared to the corresponding motor speeds,  $f_s$ , for the (a) T200 thruster and (c) Sandshark UUV, and the desired speed for (b) the Riptide vehicle. The predicted sideband spacings are in dashed black. In (b) and (c), lines are drawn to show measured sideband spacings versus the true vehicle speed in the field experiments.

Furthermore, if DEMON measurements are observable, they can be used to verify these values.

The radiated noise of the UUVs was measured in the Charles River, which is a shallow water environment with dynamic and loud ambient noise from passing boats, construction, and motor vehicle traffic on bridges. The UUV propeller rotation frequency was extrapolated by measuring the associated harmonics of the  $f_{PWM}$  carrier. In the case of the Sandshark, where the turn-per-knot ratio is known, the vehicle speed was predicted with 1.3% accuracy and within the error range of the INS reported speed. As demonstrated in the field tests, measuring the motor noise signature has several advantages over the DEMON method: simplicity (in

regards to choosing an optimal passband for cavitation noise), a higher SNR, and an omni-directional radiation pattern. Furthermore, when boats passed by the UUV, the motor noise is still observable, but the DEMON spectrum is dominated by the interfering boat's propeller cavitation noise. Because the radiation pattern due to machinery vibration depends on how the machinery (the motor in the case) is mounted to the hull, we predict that a large section of the UUV hull is vibrating at the motor tones we observe. This path of vibration from the motor to the water could explain the omni-directional pattern of noise and high SNR. Understanding the origins of acoustic noise in these autonomous platforms can inform quieter UUV propulsion design to avoid interference with onboard sensors and disturbance to marine life for wildlife monitoring applications. By predicting the potential electromagnetic vibration frequencies, the mechanical system can be designed to avoid structural resonance. Vibration isolation mounts could also be installed to minimize the paths of vibration to the hull. In the future, based off of these findings, quieting techniques for BLDC motors in UUVs can be compared and assessed, particularly for mitigating  $f_{PWM}$ .

Another important application of this work is passively tracking UUVs. A BLDC motor-powered vehicle can be detected and classified by its unique acoustic signature of high frequency harmonics of  $f_{PWM}$ . As shown with the case of the Sandshark, extrapolating  $f_s$  from motor noise can be utilized for speed estimation, if the turn-per-knot ratios are known. A next step for this research is to incorporate target motion analysis, which will be the primary focus of our follow-up work. The extensive research done in UUV navigation, summarized in Liam *et al.*, can be leveraged for selecting a state estimate technique.<sup>38</sup> To extend this work to other vehicles and environments with non-negligible currents, a combination of dynamic and kinematic models, with current velocity in the state vector, have been demonstrated with success.<sup>39–41</sup> Furthermore, in cases where there are multiple marine vessels present, like ship traffic and UUVs, multi-source tracking could be investigated. Using the micro-UUV signatures obtained experimentally, passively tracking the motor noise under various environmental conditions can be assessed.

In conclusion, we have experimentally identified acoustic features in two micro-UUVs and a thruster in isolation, which we found to originate from the BLDC motor in their respective propulsion systems. These findings have the potential to inform future designs of marine robotic platforms that also rely on off-the-shelf BLDC motors and are used for low-noise applications like tracking marine life. Last, these results can be used to improve target motion analysis applied to UUVs.

## ACKNOWLEDGMENTS

The authors thank members of the Laboratory for Autonomous Marine Sensing Systems, MIT Towing Tank, and the MIT sailing pavilion staff for experimental support,



especially: Oscar Viquez, Erin Fischell, Nick Rypkema, Supun Randeni, Rui Chen, Eeshan Bhatt, Bradli Crump, Dan Goodwin, Greg Nannig, Michael Novitzky, and Miranda Kotidis. The authors are grateful for discussions with Hilary Johnson, Daniel Frey, Steven Leeb, Dani Goldberg, and Joel Parry. This work was supported by the Office of Naval Research (Award No. N00014-17-1-2474), DARPA, the Draper Fellowship, and the National Defense Science and Engineering Graduate Fellowship Program.

- <sup>1</sup>C. J. McFarland, M. V. Jakuba, S. Suman, J. C. Kinsey, and L. L. Whitcomb, "Toward ice-relative navigation of underwater robotic vehicles under moving sea ice: Experimental evaluation in the arctic sea," in *Proceedings of IEEE International Conference on Robotics and Automation (ICRA)* (2015), pp. 1527–1534.
- <sup>2</sup>J. C. Kinsey, D. R. Yoerger, M. V. Jakuba, R. Camilli, C. R. Fisher, and C. R. German, "Assessing the Deepwater Horizon oil spill with the Sentry autonomous underwater vehicle," in *Proceedings of IEEE/RSJ International Conference on Intelligent Robots and Systems* (2011), pp. 261–267.
- <sup>3</sup>P. F. Lermusiaux, T. Lolla, P. J. Haley, Jr., K. Yigit, M. P. Ueckermann, T. Sondergaard, and W. G. Leslie, "Science of autonomy: Time-optimal path planning and adaptive sampling for swarms of ocean vehicles," in *Springer Handbook of Ocean Engineering* (Springer, 2016), pp. 481–498.
- <sup>4</sup>M. Eckstein, "DARPA, BAE systems developing small unmanned underwater vehicles to hunt enemy submarines," US Naval Institute News, **2017**, 1–8.
- <sup>5</sup>"Large displacement unmanned underwater vehicle innovative naval prototype technology," Office of Naval Research ONRBAA Announcement 11-025 (2011).
- <sup>6</sup>M. Eckstein, "Navy hosts virtual industry day to keep Hammerhead mine on accelerated acquisition path," US Naval Institute News **2010**, 1–10.
- <sup>7</sup>"Counter-unmanned undersea vehicle (C-UUV) hosted by the Stiletto Maritime Demonstration Program, capability demonstration 17-1," ASD Rapid Reaction Technology Office CD17-1, 1–8 (2016).
- <sup>8</sup>DARPA, "Special notice DARPA-SN-16-11 1: Open ocean counter unmanned underwater vehicle (OOCUUV) study," 1–7 (2016).
- <sup>9</sup>"Unmanned undersea vehicle (UUV) detection and classification in harbor environments," Office of Naval Research (ONR). Small Business Innovation Research (SBIR) Proposal Submission (2015).
- <sup>10</sup>K. W. Chung, A. Sutin, A. Sedunov, and M. Bruno, "DEMON acoustic ship signature measurements in an urban harbor," *Adv. Acoust. Vibration* **2011**, 952798.
- <sup>11</sup>A. Pollara, A. Sutin, and H. Salloum, "Improvement of the Detection of Envelope Modulation on Noise (DEMON) and its application to small boats," in *Proceedings of OCEANS MTS/IEEE*, Monterey, CA (2016).
- <sup>12</sup>G. L. Ogden, L. M. Zurk, M. E. Jones, and M. E. Peterson, "Extraction of small boat harmonic signatures from passive sonar," *J. Acoust. Soc. Am.* **129**(6), 3768–3776 (2011).
- <sup>13</sup>W. C. Dixon and C. R. Rollins, "Very low frequency acoustic detection of submarines," Naval Research Laboratory (1977).
- <sup>14</sup>Robert J. Urick, *Principles of Underwater Sound* (Peninsula Publishing, 1983).
- <sup>15</sup>S. Stanic, C. Kirkendall, A. Tveten, and T. Barock, "Passive swimmer detection," *NRL Rev.: Acoust.* **2004**, 97–98.
- <sup>16</sup>L. Fillinger, P. de Theije, M. Zampolli, A. Sutin, H. Salloum, N. Sedunov, and A. Sedunov, "Towards a passive acoustic underwater system for protecting harbours against intruders," in *Proceedings of International WaterSide Security Conference* (2010), pp. 1–7.
- <sup>17</sup>A. Sutin, B. Bunin, A. Sedunov, N. Sedunov, L. Fillinger, M. Tsionskiy, and M. Bruno, "Stevens passive acoustic system for underwater surveillance," in *Proceedings of International WaterSide Security Conference* (2010), pp. 1–6.
- <sup>18</sup>M. H. A. d'Assumpcao, "Theoretical assessment of 'DEMON' Performance," Department of Supply Australian Defense Scientific Service Weapons Research Establishment, Technical Memorandum CPD no. 169.
- <sup>19</sup>N. De Moura, J. De Seixas, and R. Ramos, "Passive sonar signal detection and classification based on independent component analysis," in *Sonar Systems* (InTech, 2011), pp. 93–103.
- <sup>20</sup>J. D. Holmes, W. M. Carey, and J. F. Lynch, "An overview of unmanned underwater vehicle noise in the low to mid frequencies bands," in *Proceedings of Meetings on Acoustics 159ASA* (2010) Vol. 9, p. 065007.
- <sup>21</sup>J. Gebbie, M. Siderius, and J. S. Allen III, "Aspect-dependent radiated noise analysis of an underway autonomous underwater vehicle," *J. Acoust. Soc. Am.* **132**(5), EL351–EL357 (2012).
- <sup>22</sup>S. Zhang and X. Ma, "A speed measurement method using AUV radiated noise spectrum," in *Proceedings of OCEANS-MTS/IEEE Kobe Techno-Oceans (OTO)* (2018), pp. 1–5.
- <sup>23</sup>R. Wynn, E. Linley, and J. Hunt, "Global inventory of AUV and glider technology available for routine marine surveying," in *United Kingdom Research and Innovation Natural Environment Research Council: Marine Renewable Energy Knowledge Exchange Programme. Appendix 1* (2013), pp. 16–153.
- <sup>24</sup>G. Griffiths, P. Enoch, and N. W. Millard, "On the radiated noise of the Autosub autonomous underwater vehicle," *ICES J. Marine Sci.* **58**(6), 1195–1200 (2001).
- <sup>25</sup>R. W. Button, J. Kamp, T. B. Curtin, and J. Dryden, "A survey of missions for unmanned undersea vehicles," Technical Report, RAND National Defense Research Institute (2009).
- <sup>26</sup>W. Lo, C. C. Chan, Z.-Q. Zhu, L. Xu, D. Howe, and K. Chau, "Acoustic noise radiated by PWM-controlled induction machine drives," *IEEE Trans. Indust. Electron.* **47**(4), 880–889 (2000).
- <sup>27</sup>H. J. Lee, S. U. Chung, and S. M. Hwang, "Noise source identification of a BLDC motor," *J. Mech. Sci. Technol.* **22**(4), 708–713 (2008).
- <sup>28</sup>I. Tsoumas, H. Tischmacher, and B. Eichinger, "Influence of the number of pole pairs on the audible noise of inverter-fed induction motors: Radial force waves and mechanical resonances," in *Proceedings of 2014 International Conference on Electrical Machines (ICEM)* (2014), pp. 1811–1817.
- <sup>29</sup>E. Zeze and K. Akatsu, "Research on vibration analysis and noise-reduction technique of PM motor," in *Proceedings of 20th International Conference on Electrical Machines* (2012), pp. 458–463.
- <sup>30</sup>J. Le Besnerais, V. Lanfranchi, M. Hecquet, and P. Brochet, "Characterization and reduction of audible magnetic noise due to PWM supply in induction machines," *IEEE Trans. Indust. Electron.* **57**(4), 1288–1295 (2009).
- <sup>31</sup>M. S. Islam, R. Islam, and T. Sebastian, "Noise and vibration characteristics of permanent-magnet synchronous motors using electromagnetic and structural analyses," *IEEE Trans. Indust. Appl.* **50**(5), 3214–3222 (2014).
- <sup>32</sup>T. Hara, T. Ajima, Y. Tanabe, M. Watanabe, K. Hoshino, and K. Oyama, "Analysis of vibration and noise in permanent magnet synchronous motors with distributed winding for the PWM method," *IEEE Trans. Indust. Appl.* **54**(6), 6042–6049 (2018).
- <sup>33</sup>D. G. Dorrell, M.-F. Hsieh, M. Popescu, L. Evans, D. A. Staton, and V. Grout, "A review of the design issues and techniques for radial-flux brushless surface and internal rare-earth permanent-magnet motors," *IEEE Trans. Indust. Electron.* **58**(9), 3741–3757 (2010).
- <sup>34</sup>T. G. Habetler and D. M. Divan, "Acoustic noise reduction in sinusoidal PWM drives using a randomly modulated carrier," *IEEE Trans. Power Electron.* **6**(3), 356–363 (1991).
- <sup>35</sup>A. Lelkes, J. Krotsch, and R. W. De Doncker, "Low-noise external rotor BLDC motor for fan applications," in *Proceedings of the 2002 IEEE Industry Applications Conference. 37th IAS Annual Meeting (Cat. No. 02CH37344)* (2002), Vol. 3, pp. 2036–2042.
- <sup>36</sup>P. Welch, "The use of fast Fourier transform for the estimation of power spectra: A method based on time averaging over short, modified periodograms," *IEEE Trans. Audio Electroacoust.* **15**(2), 70–73 (1967).
- <sup>37</sup>M. R. Benjamin, H. Schmidt, P. M. Newman, and J. J. Leonard, "Nested autonomy for unmanned marine vehicles with MOOS-IvP," *J. Field Robotics* **27**(6), 834–875 (2010).
- <sup>38</sup>L. Paull, S. Saeedi, M. Seto, and H. Li, "AUV navigation and localization: A review," *IEEE J. Oceanic Engineer.* **39**(1), 131–149 (2014).
- <sup>39</sup>B. Allotta, R. Costanzi, F. Fanelli, N. Monni, L. Paolucci, and A. Ridolfi, "Sea currents estimation during AUV navigation using Unscented Kalman Filter," *IFAC-PapersOnLine* **50**(1), 13668–13673 (2017).
- <sup>40</sup>S. A. Randeni, P. A. L. Forrest, R. Cossu, Z. Q. Leong, and D. Ranmuthugala, "Determining the horizontal and vertical water velocity components of a turbulent water column using the motion response of an autonomous underwater vehicle," *J. Marine Sci. Engineer.* **5**(3), 25 (2017).
- <sup>41</sup>Ø. Hegrenæs and O. Hallingstad, "Model-aided INS with sea current estimation for robust underwater navigation," *IEEE J. Oceanic Engineer.* **36**(2), 316–337 (2011).